RESEARCH ARTICLE | OCTOBER 25 2024

Weyl points in a twisted multilayer photonic system

Aivar Abrashuly ; Cheng Guo ; Georgia T. Papadakis ; Peter B. Catrysse ; Shanhui Fan

Appl. Phys. Lett. 125, 171703 (2024)
https://doi.org/10.1063/5.0231392

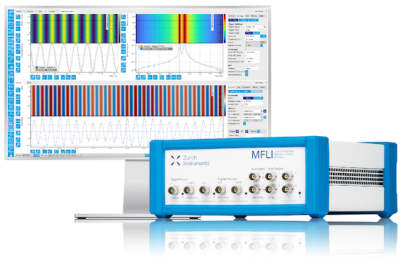

Applied Physics Letters ARTICLE pubs.aip.org/aip/apl

Weyl points in a twisted multilayer photonic system

Cite as: Appl. Phys. Lett. **125**, 171703 (2024); doi: 10.1063/5.0231392
Submitted: 30 July 2024 · Accepted: 9 October 2024 ·
Published Online: 25 October 2024

View Online Export Citation CrossMark

Aivar Abrashuly,[1] Cheng Guo,[1] Georgia T. Papadakis,[2] Peter B. Catrysse,[1] and Shanhui Fan[1,a)]

AFFILIATIONS

[1]Ginzton Laboratory and Department of Electrical Engineering, Stanford University, Stanford, California 94305, USA
[2]ICFO - Institut de Ciencies Fotoniques, The Barcelona Institute of Science and Technology, 08860 Castelldefels, Barcelona, Spain

[a)]Author to whom correspondence should be addressed: shanhui@stanford.edu

ABSTRACT

We numerically demonstrate the creation of Weyl points in a twisted multilayer photonic system. In our system, each layer is anisotropic with plasmonic response along a direction perpendicular to the layer and with anisotropic dielectric response within the layer. We show that Weyl points can be created by controlling the twist angles between the layers so that spatial-inversion symmetry is broken. Compared with existing approaches, our findings offer a potentially simpler structure for creating Weyl points and highlight the prospect of using twisted multilayer systems for achieving topological photonic effects.

A Weyl point is a twofold degenerate point in a three-dimensional band structure that carries a non-zero topological charge.[1] It is a monopole of the Berry curvature field and is robust to small perturbations. In the past decade, the physics associated with Weyl points has been extensively investigated in both electronic[2,3] and photonic[4–7] systems. The exploration of Weyl point physics in photonic systems is of fundamental interest since the physics of photons can be fundamentally different from, and hence complementary to, that of electrons.[8] On the one hand, the manifestation of Weyl point physics in electronic systems that involve either the charge or the fermionic nature of electrons does not have direct photonic analog. On the other hand, Weyl points in photonic systems find potential applications including large-area single-mode lasers[9] and angular filters for light,[10] which have no direct electronic counter parts.

Creating a Weyl point requires breaking either time-reversal or spatial-inversion symmetry.[11] For example, a Weyl point can be achieved in a uniform magnetized plasma that breaks the time-reversal symmetry, but the requirement for a large external magnetic field limits the usefulness of this approach for potential applications.[4] Alternatively, a Weyl point has been designed and observed in three-dimensional reciprocal photonic crystals or metamaterials that break spatial-inversion symmetry.[8] However, the geometries of these photonic crystals or metamaterials are rather complex and are difficult to implement, especially in the optical frequency range.

In this paper, we show that a Weyl point can be achieved in a much simpler twisted multilayer photonic system (Fig. 1). In this system, each of the layers is described by an anisotropic permittivity tensor. One of the principal axes is perpendicular to the layer, and the corresponding permittivity component along this direction is described by the Drude model. The other two principal axes are in-plane and, thus, parallel to the interfaces between the layers. The corresponding permittivity along these two orthogonal directions is both positive and non-dispersive. In such a multilayer system, one can choose the twist angle between layers to break spatial-inversion symmetry. We show that with a suitable choice of twist angles, this photonic system exhibits Weyl points.

We note that in recent years, there have been significant activities in the experimental exploration of physics and device applications of twisted multilayer systems.[12–17] Our work points to topological photonic band structures that can be synthesized in these twisted multilayer systems.

Figure 1 shows our proposed design of a periodic multilayer structure. The unit cell of the structure is comprised of three layers made of identical materials. The thickness of each layer is the same and equal to $L = a/3$, where a is the length of the unit cell. Each layer consists of a homogeneous medium with the relative permeability $\mu_r = 1$. The first layer in each unit cell is described by an electric permittivity of the form:

$$\overleftrightarrow{\varepsilon}_r^{(1)} = \mathrm{diag}\{\varepsilon_x, \varepsilon_y, \varepsilon_z\}. \quad (1)$$

The x and y axes are in-plane with each layer, while the z axis is perpendicular to the layer. The permittivity components along the x- and

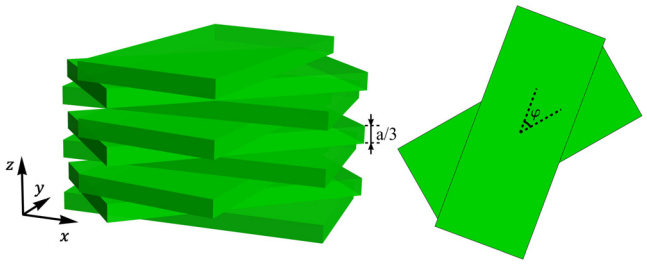

FIG. 1. Twisted periodic multilayer photonic system. Each unit cell has a thickness a and consists of three layers. Within each unit cell, a layer is azimuthally twisted with respect to the layer below by an angle φ. Each layer is represented by a block with the directions of the edges of the block corresponding to the principal axes for its permittivity tensor.

y-directions, i.e., ε_x and ε_y, are both positive but differ from each other. Along the z-direction, the medium possesses a plasmonic response with a Drude dispersion model ($\varepsilon_z = 1 - \omega_p^2/\omega^2$), where ω_p represents the plasma frequency. In the paper, for illustration purposes, we choose $\omega_p = 0.25 \cdot \frac{2\pi c}{a}$, $\epsilon_x = 2.2$, and $\epsilon_y = 1.2$. Also, throughout the paper, the angular frequencies are in the unit of $2\pi c/a$, and the wavevectors are in the unit of $2\pi/a$.

To observe a Weyl point in the band structure, it is necessary to break either time-reversal or spatial-inversion symmetry. In our system, we break spatial-inversion symmetry with the design of the 3-layer unit cell such that the second and third layers within the cell are azimuthally rotated with respect to the first layer by angles φ and 2φ, respectively. This angle φ can be chosen arbitrarily, as long as the inversion symmetry is broken. In the coordinate system as indicated in Fig. 1, the permittivity tensor of the three layers can be represented by $\overleftrightarrow{\varepsilon}_r^{(i)} = R_z(\varphi)^{i-1} \cdot \overleftrightarrow{\varepsilon}_r^{(1)} \cdot R_z(\varphi)^{-(i-1)}$, where $i = 1, 2, 3$. The rotation matrix is as follows:

$$R_z(\varphi) = \begin{pmatrix} \cos\varphi & -\sin\varphi & 0 \\ \sin\varphi & \cos\varphi & 0 \\ 0 & 0 & 1 \end{pmatrix}. \tag{2}$$

To understand the photonic band structure of the system in Fig. 1, we first recall the band structure of a uniform system as described by Eq. (1). Along the z-axis, uniform system supports three modes: a longitudinal mode at a constant frequency $\omega = \omega_p$, since $\varepsilon_z = 0$ at this frequency, and two transverse modes. The longitudinal mode has an electric field that is non-zero only along the z axis. The two transverse modes supported are not degenerate since $\varepsilon_x \neq \varepsilon_y$. The longitudinal mode and the transverse modes cross at the crossing wavevectors of $k_{c1} = 0.31$ and $k_{c2} = 0.35$, respectively. At these wavevectors, the bands are twofold degenerate.

To calculate the propagating modes inside the twisted multilayer photonic system shown in Fig. 1, we use the transfer-matrix method.[18] For each layer, from Maxwell's equations, we derive four coupled differential equations that govern the (transverse) wave propagation in the system,

$$\frac{d}{dz} f(z) = iP \cdot f(z), \tag{3}$$

where $f(z) = \left[E_x(z), E_y(z), H_x(z), H_y(z)\right]^T$ is the in-plane electromagnetic field at point z. For the first layer, we have

$$P = \begin{pmatrix} 0 & 0 & \frac{k_x k_y}{\varepsilon_z \omega^2} & 1 - \frac{k_x^2}{\varepsilon_z \omega^2} \\ 0 & 0 & -1 + \frac{k_y^2}{\varepsilon_z \omega^2} & -\frac{k_x k_y}{\varepsilon_z \omega^2} \\ -\frac{k_x k_y}{\omega^2} & -\varepsilon_y + \frac{k_x^2}{\omega^2} & 0 & 0 \\ \varepsilon_x - \frac{k_y^2}{\omega^2} & \frac{k_x k_y}{\omega^2} & 0 & 0 \end{pmatrix}, \tag{4}$$

where k_x and k_y are the x and y components of the wavevector $k_{||}$ parallel to the layers, respectively. Integration of Eq. (3) allows us to obtain the transfer matrix of the first layer. The transfer matrix of other layers can be obtained similarly using rotation matrices. The band structure of the system can then be obtained from these transfer matrices. Since f only contains in-plane fields, the formalism does not incorporate the contributions of the longitudinal mode when $k_x = k_y = 0$. On the other hand, the impact of the longitudinal mode can be studied with this formalism by examining the cases with small k_x and k_y, since in these cases, the longitudinal mode hybridizes with the transverse modes, and, thus, all modes have in-plane field components. Moreover, since k_x and k_y are small, the degree of hybridization is also small. Thus, the hybridized modes can be referred to as quasi-transverse and quasi-longitudinal modes, depending on whether the transverse or the longitudinal field components dominate, respectively.

The photonic band structure of ω as a function of k_z is shown in Fig. 2(b) for a specific example in which the three layers of the unit cell are azimuthally rotated by an angle $\varphi = 2\pi/9$ and with $k_{||}a = (0.05/2\pi, 0)$. The band structure exhibits a quasi-longitudinal mode near $\omega = \omega_p$ with its frequency largely independent of the perpendicular wave vector k_z. There are also two quasi-transverse modes possessing an approximately linear dispersion over much of the Brillouin Zone. The dispersions of these modes are very similar to the longitudinal and transverse modes at $k_{||} = 0$ for the uniform medium as shown in Fig. 2(a). The difference is most prominent where k_z is near the crossing wavevectors of $k_{c1} = 0.31$ and $k_{c2} = 0.35$, where the hybridization occurs. As an illustration, Fig. 2(c) shows a zoomed-in view of the band structure in the vicinity of $k_z = k_{c2}$ and $\omega = \omega_p$, which exhibits the anti-crossing between the quasi-longitudinal and the quasi-transverse modes. As $k_{||}$ approaches zero, the band structure approaches that of the uniform media at $k_{||} = 0$ as shown in Fig. 2(a).

In Fig. 3, we provide a more detailed illustration of the photonic band structure in the vicinity of $\boldsymbol{k} = (0, 0, k_{c2})$ near $\omega = \omega_p$. The dispersions along the k_x and k_y axes are linear with very similar slopes, resulting in a cone-shaped dispersion in the $\omega - k_x - k_y$ space as shown in Fig. 3(a). In Figs. 3(b) and 3(c), we observe the crossing of a flatband and a linear dispersion band along the k_x-axis. Such crossing forms degenerate points. The degeneracy is lifted away from the k_z axis. The results indicate that the twofold degeneracy between the longitudinal and the transverse modes at $k_{||} = 0$ is lifted for small non-zero $k_{||}$ due to the hybridization as induced by the twist between the layers, resulting in the creation of Weyl points in the band structure. The dispersion of the Weyl point here lies at the boundary between Type-I and Type-II Weyl points.

The dispersion shown in Figs. 2 and 3 can be described by an effective Hamiltonian that is applicable in the vicinity of a Weyl point:[19]

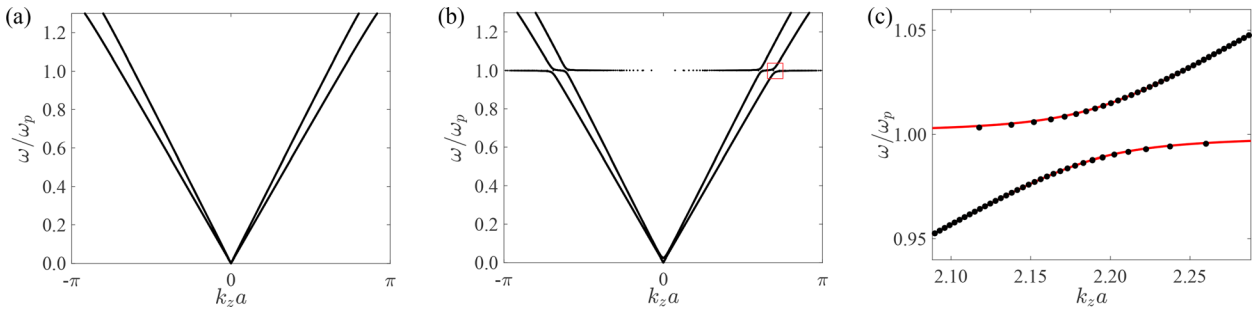

FIG. 2. The photonic band structure along the z direction of the system shown in Fig. 1 for an angle $\varphi = 2\pi/9$. (a) $k_{||} = (0, 0)$. This band structure is also nearly the same as that of the uniform system as described by Eq. (1). Two black lines represent transverse x and y modes, while the red line represents longitudinal mode at $\omega = \omega_p$. (b) $k_{||} = (0.05/2\pi, 0)$. (c) The scaled view of the same band structure inside the red rectangle in Fig. 2(a). The black dots are obtained from the transfer-matrix method, and the red line is a fit using Eq. (6) with the parameters of $\alpha_1 = 1.29 \times 10^{-1}$, $\alpha_2 = 9.08 \times 10^{-2}$, and $\beta = 2.28$.

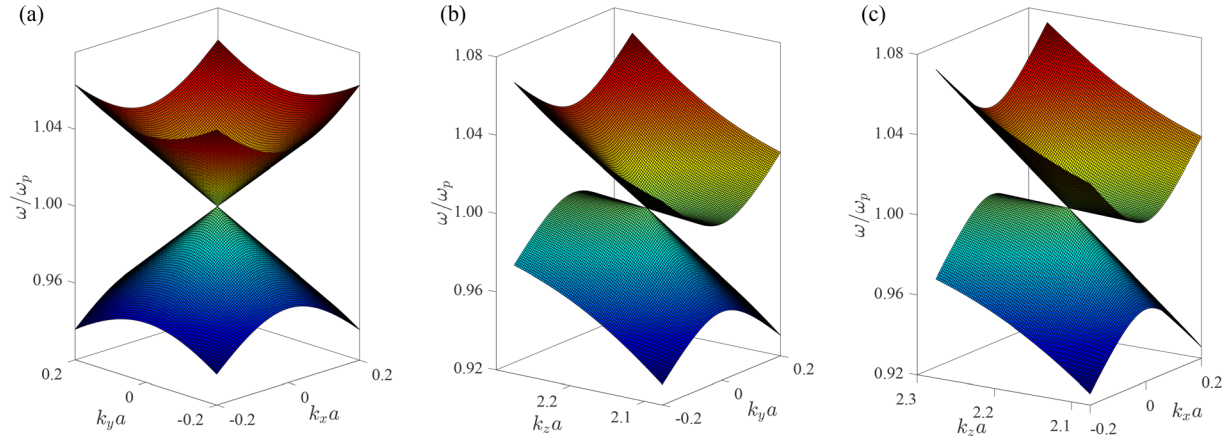

FIG. 3. (a) The dispersion in the $k_x - k_y$ plane at $k_z = k_c = 0.35$. (b) The dispersion in the $k_x - k_z$ plane at $k_y = 0$. (c) The dispersion in the $k_y - k_z$ plane at $k_x = 0$. The dispersion is linear along all the directions, indicating the crossing point is a Weyl point.

$$\boldsymbol{H}_{\mathbf{eff}} = \nu_x \delta k_x \boldsymbol{\sigma}_{\mathbf{x}} + \nu_y \delta k_y \boldsymbol{\sigma}_{\mathbf{y}} + \nu_z \delta k_z (\boldsymbol{\sigma}_{\mathbf{z}} + \tau \mathbf{I}). \tag{5}$$

Here, ν_i, $i = x$, y, and z are group velocities in the x, y, and z directions, respectively. $\boldsymbol{\sigma_i}$ s are the Pauli matrices. $(\delta k_x, \delta k_y, \delta k_z)$ are the displacement of the wavevectors from the wavevector of the Weyl point. Equation (5) is the simplest form of a two-band Hamiltonian that exhibits a Weyl point of a charge of \pm 1. In our case, since the Weyl point is located at a wavevector $(0, 0, k_c)$, we have $\delta k_x = k_x$, $\delta k_y = k_y$, $\delta k_z = k_z - k_c$. $\tau = \pm 1$ is used to describe the specific case of a Weyl point at the transition between Types I and II Weyl points. The eigenvalues of Eq. (5) describe $\delta\omega = \omega - \omega_c$, i.e., the deviation of the eigenfrequency ω from the frequency of the Weyl point ω_c. From Eq. (5), for $\tau = \pm 1$, we have

$$\delta k_z \delta\omega = -\alpha_1 k_x^2 - \alpha_2 k_y^2 + \beta \delta\omega^2, \tag{6}$$

where $\alpha_x = \nu_x^2/(2\nu_z)$, $\alpha_y = \nu_y^2/(2\nu_z)$, and $\beta = 1/(2\nu_z)$.[10] In Fig. 2(b), we show an excellent fit of this equation with the band structure obtained using the transfer-matrix method, which validates the use of effective Hamiltonian of Eq. (5) for our system.

A key signature of a Weyl point is its topological charge. For our system, we calculate the topological charge of the Weyl point by integrating the Berry connection along various loops in the wavevector space centered around the Weyl point, as shown in Fig. 4.[19] For this purpose, we consider N equally spaced wavevector points on a loop and compute

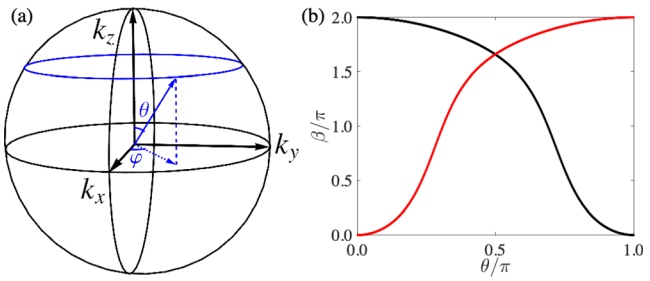

FIG. 4. (a) Schematic diagram of momentum space illustrating the charge of a Weyl point. The center of the sphere is the Weyl point in momentum space. The Berry phase is calculated along the blue loop of constant θ. (b) The flux of Berry curvature as a function of θ for two crossing bands in Fig. 2(a) for the Weyl point near $k_z = k_{c1}$ in Fig. 2(a). The red and black curves correspond to lower and upper bands, respectively.

$$\beta = -\mathrm{Im}\ln\left[\langle\psi_0|\psi_1\rangle\langle\psi_1|\psi_2\rangle\ldots\langle\psi_{N-1}|\psi_0\rangle\right], \tag{7}$$

where $|\psi_i\rangle$ is the eigenstate in one of the bands at the ith wavevector point. The inner product $\langle\psi_i|\psi_j\rangle$ is defined as

$$\langle\psi_i|\psi_j\rangle = \int dz \frac{1}{2}\left[\mathbf{E}_i^*(z)\cdot\frac{\varepsilon_0\partial(\omega\varepsilon_r(z))}{\partial\omega}\mathbf{E}_j(z) + \mathbf{H}_i^*(z)\cdot\mu_0\mathbf{H}_j(z)\right], \tag{8}$$

where $\mathbf{E}_i$ and $\mathbf{H}_i$ are the electric and magnetic fields for the eigenstate, respectively, and the integration occurs over a single unit cell. We choose the normalization such that $\langle\psi_i|\psi_i\rangle = 1$. The result of this calculation corresponds to the integration of the Berry curvature flux through the loop. The computational procedure here is the same as that for electronic systems, except that inner product in Eq. (8) utilizes the electromagnetic fields of eigenmodes in the photonic system. In Fig. 4(b), we plot the Berry curvature flux thus computed, for a set of loops with constant k_z. As the k_z sweeps through the Weyl point at k_{c1}, the Berry curvature flux varies from 0 to 2π for the upper band. The calculation indicates that the Weyl point here has a topological charge of $+1$, consistent also with the prediction of the effective Hamiltonian of Eq. (5). The same calculation for the Weyl point at k_{c2} reveals that it has a topological charge of -1.

From time-reversal symmetry, the system also supports two Weyl points at $k_z = -k_{c1}$ and $-k_{c2}$. The charges of these two Weyl points are the same as those at $k_z = k_{c1}$ and $k_z = k_{c2}$, respectively. Thereby, for this periodic system, the total charge of all four Weyl points inside the Brillouin zone presented in Fig. 2(a) vanishes. We have verified that there are no other Weyl points at higher frequencies. The vanishing of the total charge of the Weyl points is consistent with Ref. 19.

As discussed in previous paragraphs, the Weyl point in this photonic system lies at the transition between Types I and II Weyl points. To control the transition between these two types, one can add a nonlocal effect to the permittivity along the z axis [$\varepsilon_z = \varepsilon_z(\omega, k_z)$], as discussed in Ref. 8. In this case, the longitudinal mode in the band structure of Fig. 2(a) is no longer flat. Depending on the slope of the longitudinal mode, the Weyl points become either type-I, with an ellipsoidal isofrequency surface around the Weyl point, or type-II, with a hyperbolic constant frequency surface. Furthermore, since the Weyl points are separated along the k_z axis, the Fermi arc that connects two pairs of Weyl points should appear by truncating the structure on the xz or yz planes.

Finally, we note that emerging materials with highly anisotropic properties can serve as a material platform for practical realization of the proposed concept. In particular, the permittivity tensor in Eq. (1) can be realized with α-MoO_3, a bi-axial crystal with the Reststrahlen band, where ε_x and ε_y are positive but different from each other, and ε_z is near zero.[20,21] Also, while in our work, the unit cell consists of three layers of equal thickness, Weyl points can also be achieved with a unit cell with two layers, with appropriate choice of layer thickness that are not equal. Alternatively, the permittivity tensor in Eq. (1) can be achieved in a metamaterial consisting of a two-dimensional lattice of metal wires, possessing hyperbolic dispersion. In the effective medium regime,[22–24] such a system has a plasmonic response along the wires and a dielectric response perpendicular to the wires. The in-plane anisotropy in its dielectric response can be achieved with a proper choice of the geometry of either the lattice or the cross section of the wires.

In summary, we showed that a Weyl point can be achieved in a twisted periodic multilayer photonic system, in which the layers are described by an anisotropic permittivity tensor with anisotropic dielectric in-plane response and plasmonic Drude response perpendicular to the layers. The twist between the layers breaks spatial-inversion symmetry, resulting in Weyl points. Our work points to topological photonic band structures that can be synthesized in twisted multilayer systems. The multilayer geometry of our design, which can be implemented without the use of lithography, may facilitate the application of Weyl point physics in large-area devices such as high-power single-mode lasers or angular filters.

This work was supported by an MURI project from the U.S. Air Force Office of Scientific Research (Grant No. FA9550-21-1-0244) and by the U.S. Department of Energy (Grant No. DE-FG02-07ER46426).

AUTHOR DECLARATIONS

Conflict of Interest

The authors have no conflicts to disclose.

Author Contributions

Aivar Abrashuly: Investigation (equal); Methodology (equal); Resources (equal); Software (equal); Visualization (equal); Writing – original draft (equal); Writing – review & editing (equal). **Cheng Guo:** Project administration (equal); Software (equal); Writing – review & editing (equal). **Georgia T. Papadakis:** Project administration (equal); Software (equal); Writing – review & editing (equal). **Peter B. Catrysse:** Project administration (equal); Writing – review & editing (equal). **Shanhui Fan:** Methodology (equal); Project administration (equal); Supervision (equal); Validation (equal); Writing – original draft (equal); Writing – review & editing (equal).

DATA AVAILABILITY

The data that support the findings of this study are available from the corresponding author upon reasonable request.

REFERENCES

[1]H. Weyl, "Elektron und gravitation. I," Z. Phys. **56**, 330 (1929).
[2]S.-Y. Xu, I. Belopolski, N. Alidoust *et al.*, "Discovery of a Weyl fermion semimetal and topological Fermi arcs," Science **349**, 613 (2015).
[3]B. Q. Lv, H. M. Weng, B. B. Fu *et al.*, "Experimental discovery of Weyl semimetal TaAs," Phys. Rev. X **5**, 031013 (2015).
[4]W. Gao, B. Yang, M. Lawrence, F. Fang, B. Béri, and S. Zhang, "Photonic Weyl degeneracies in magnetized plasma," Nat. Commun. **7**, 12435 (2016).
[5]L. Lu, L. Fu, J. D. Joannopoulos, and M. Soljačić, "Weyl points and line nodes in gyroid photonic crystals," Nat. Photonics **7**, 294 (2013).
[6]L. Lu, Z. Wang, D. Ye, L. Ran, L. Fu, J. D. Joannopoulos, and M. Soljačić, "Experimental observation of Weyl points," Science **349**, 622 (2015).
[7]M.-L. Chang, M. Xiao, W.-J. Chen, and C. T. Chan, "Multiple Weyl points and the sign change of their topological charges in woodpile photonic crystals," Phys. Rev. B **95**, 125136 (2017).
[8]M. Xiao, Q. Lin, and S. Fan, "Hyperbolic Weyl point in reciprocal chiral metamaterials," Phys. Rev. Lett. **117**, 057401 (2016).
[9]S.-L. Chua, L. Lu, J. Bravo-Abad, J. D. Joannopoulos, and M. Soljačić, "Larger-area single-mode photonic crystal surface-emitting lasers enabled by an accidental Dirac point," Opt. Lett. **39**, 2072 (2014).

[10]Y. Shen, D. Ye, I. Celanovic, S. G. Johnson, J. D. Joannopoulos, and M. Soljačić, "Optical broadband angular selectivity," Science **343**, 1499 (2014).
[11]C. Guo, V. S. Asadchy, B. Zhao, and S. Fan, "Light control with Weyl semimetals," eLight **3**, 2 (2023).
[12]B. Lou, N. Zhao, M. Minkov, C. Guo, M. Orenstein, and S. Fan, "Theory for twisted bilayer photonic crystal slabs," Phys. Rev. Lett. **126**, 136101 (2021).
[13]V. A. Chistyakov, V. S. Asadchy, S. Fan, A. Alù, and A. Krasnok, "Tunable magnetless optical isolation with twisted Weyl semimetals," Nanophotonics **12**, 3333 (2023).
[14]G. Hu, Q. Ou, G. Si *et al.*, "Topological polaritons and photonic magic angles in twisted α-MoO_3 bilayers," Nature **582**, 209 (2020).
[15]B. Lou, B. Wang, J. A. Rodríguez, M. Cappelli, and S. Fan, "Tunable guided resonance in twisted bilayer photonic crystal," Sci. Adv. **8**, eadd4339 (2022).
[16]S. Yves, Y.-G. Peng, and A. Alù, "Topological Lifshitz transition in twisted hyperbolic acoustic metasurfaces," Appl. Phys. Lett. **121**, 122201 (2022).
[17]M. Chen, X. Lin, T. H. Dinh, Z. Zheng, J. Shen, Q. Ma, H. Chen, P. Jarillo-Herrero, and S. Dai, "Configurable phonon polaritons in twisted α-MoO_3," Nat. Mater. **19**, 1307 (2020).
[18]T. G. Mackay and A. Lakhtakia, *The Transfer-Matrix Method in Electromagnetics and Optics* (Springer International Publishing, Cham, 2020).
[19]A. A. Soluyanov, D. Gresch, Z. Wang, Q. Wu, M. Troyer, X. Dai, and B. A. Bernevig, "Type-II Weyl semimetals," Nature **527**, 495 (2015).
[20]G. Álvarez-Pérez, T. G. Folland, I. Errea *et al.*, "Infrared permittivity of the biaxial van der Waals semiconductor α-MoO_3 from near- and far-field correlative studies," Adv. Mater. **32**, 1908176 (2020).
[21]J. Taboada-Gutiérrez, G. Alvarez-Perez, J. Duan *et al.*, "Broad spectral tuning of ultra-low-loss polaritons in a van der Waals crystal by intercalation," Nat. Mater. **19**, 964 (2020).
[22]X. Zhang and Y. Wu, "Effective medium theory for anisotropic metamaterials," Sci. Rep. **5**, 7892 (2015).
[23]M. G. Silveirinha, "Design of linear-to-circular polarization transformers made of long densely packed metallic helices," IEEE Trans. Antennas Propag. **56**, 390 (2008).
[24]M. G. Silveirinha, "Metamaterial homogenization approach with application to the characterization of microstructured composites with negative parameters," Phys. Rev. B **75**, 115104 (2007).